Earth and Planetary Science Letters 414 (2015) 87–99

Contents lists available at ScienceDirect

Earth and Planetary Science Letters

www.elsevier.com/locate/epsl

# Andean growth and monsoon winds drive landscape evolution at SW margin of South America

Aurélie Coudurier-Curveur [1], Robin Lacassin *, Rolando Armijo

*Institut de Physique du Globe de Paris, Sorbonne Paris Cité, Univ. Paris Diderot, UMR 7154 CNRS, France*

ARTICLE INFO

*Article history:*
Received 21 February 2014
Received in revised form 4 December 2014
Accepted 24 December 2014
Available online xxxx
Editor: Y. Ricard

*Keywords:*
Andes
landscape evolution
geomorphology
orogeny
river incision
tectonic uplift

ABSTRACT

In the Atacama Desert, the driest place on Earth located at the subduction margin of the Andes, the landscape evolves very slowly and changes in tectonic or erosion processes remain for a long time in the memory of topography. At latitude ~19°30′S, a threshold between exoreic and endoreic drainage regimes is clearly associated with the latitudinal gradient imposed by the modern monsoon (carrying humidity from the Atlantic) and disposed obliquely over catchments draining the Andes to the Pacific. We summarize the geomorphic, geological and climatic data in the threshold area. We then use these data to constrain numerical experiments of drainage evolution. Data and experimental results are consistent with the development of a flat low-energy morphology, close to sea level, interrupted at ≤10 Ma by tectonic uplift prevailing to the present suggesting trench-ward relief growth by incorporation of the coastal Atacama region to the Andes mountain belt.



## 1. Introduction

The landscape at the mountain belt flanks depends to a large extent on the competing effects of tectonic uplift, which creates vertical relief, and climate, which mediates erosion (Whittaker, 2012; Bonnet and Crave, 2003). Topography, as a filtered signal of tectonics and climate (Whittaker, 2012) is a particularly important feature that keeps a record of the changes affecting these two processes. Recent studies have demonstrated that, under constant tectonics and climate, the landscape retains limited information (Whittaker, 2012; Bonnet and Crave, 2003) and therefore traces of past perturbations become very subtle. Long-term (>1 Myr) changes are commonly assessed through proxies such as exhumation or sedimentary histories (e.g., for the Central Andes: Schildgen et al., 2007; Uba et al., 2007). However, under the hyper-arid conditions of the Atacama Desert at the west margin of the Central Andes, erosion rates are very low and time-scales of landscape evolution exceed 5 Myr (Alpers and Brimhall, 1988; Dunai et al., 2005; Nishiizumi et al., 2005; Hoke et al., 2007; Kober et al., 2007; Evenstar et al., 2009; Jordan et al., 2010). As a consequence, the landscape remains transient and well-preserved long-term effects of past changes of tectonic and erosion rates are still measurable in the topography.

The Atacama coastal morphology is marked by a conspicuous escarpment, named Coastal Scarp (CS), which limits to the West the smooth upper surface of the Coastal Cordillera (CC) and a ~100 km-wide flat surface lying at ~1 km a.s.l. at the foot of the Andean Chain (named Pampa del Tamarugal in North Chile, Figs. 1 and 2). That composite surface of Late Miocene age (e.g. Farías et al., 2005) may be traced almost continuously from ~16°S (South Peru) to ≥24°S (North Chile) for more than 1000 km (Fig. 1a), except where locally dissected by large and deep canyons (Figs. 1a and 2). In South Peru, river incision process started between 9 and 11 Ma and requires substantial continuous land uplift of similar amplitude (Schildgen et al., 2007, 2009; Schlunegger et al., 2006, 2010). Such vertical land uplift may result from ongoing tectonic processes associated with subduction (Armijo and Thiele, 1990). As in South Peru, canyon incision in North Chile is relatively young (<10 Myr) and of comparable amplitude, implying recent tectonic uplift of ~1 km (García and Hérail, 2005; Zeilinger et al., 2005; Kober et al., 2006; Kirk-Lawlor et al., 2013). By contrast, it has also been suggested that incision processes would have been triggered by climate change and coastal erosion of a pre-existent topography of mid-Tertiary age (~≥25 Ma) (e.g., Mortimer and Saric, 1975; Farías et al., 2005; García et al., 2011). In that case, the kilometric coastal uplift would be much older than the incision processes.

In order to discuss the incision mechanism in North Chile, we focus our study on a threshold area where, over a distance of less

* Corresponding author.
*E-mail address:* Lacassin@ipgp.fr (R. Lacassin).
[1] Current address: Earth Observatory of Singapore (EOS), Nanyang Technological University, Singapore.

http://dx.doi.org/10.1016/j.epsl.2014.12.047
0012-821X/

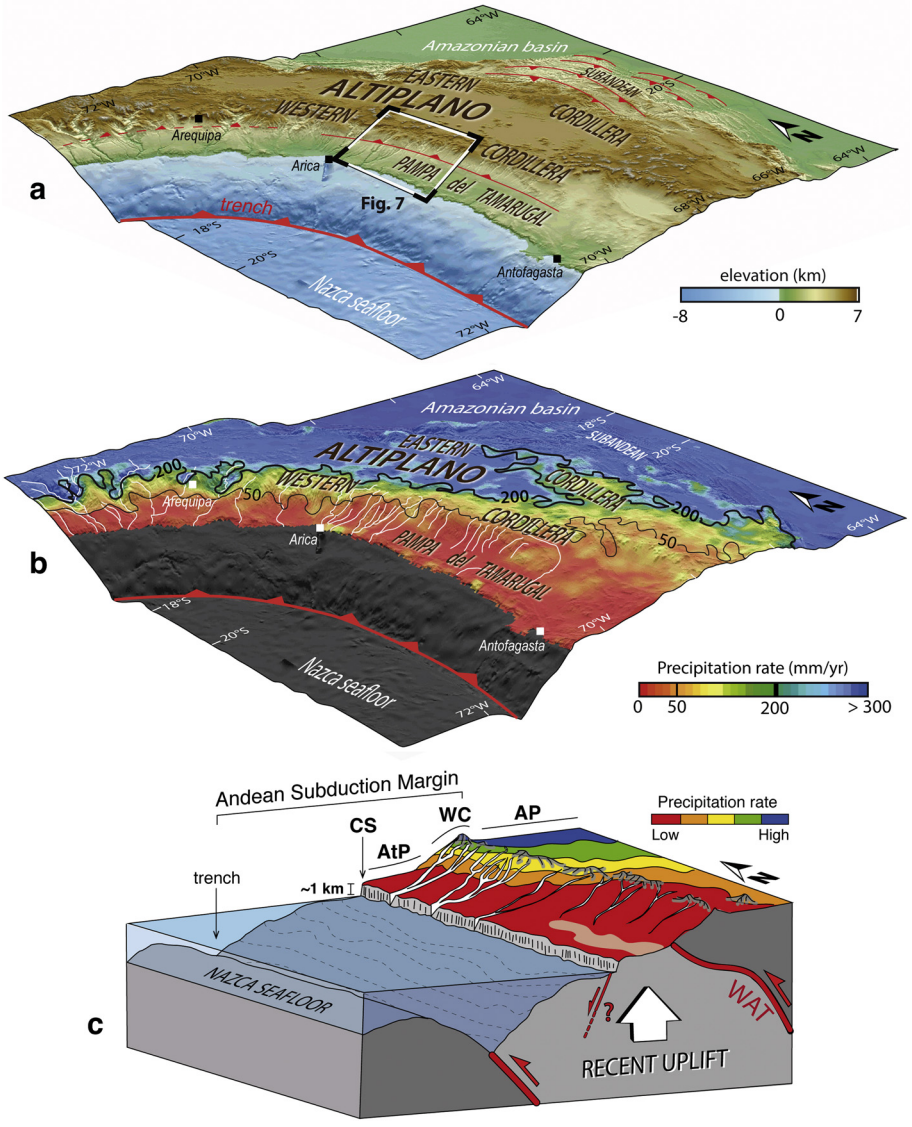


**Fig. 1.** Topography and climate of the Central Andes. (a) 3D view from SW (vertical exaggeration of 10, SRTM30+ data) displaying main Andean units. The subduction zone (trench) and frontal thrusts of Western and Eastern Cordilleras are in red. White box outlines the threshold area where drainage morphology is analyzed in detail on Fig. 8 and which corresponds to 3D sketch below. (b) Topography overlaid with present-day mean precipitation rates derived from TRMM data (see also Fig. 6). 50 and 200 mm/yr isohyets (precipitation isolines), in black, are oblique on bulk topography. The western hyper-arid region (<50 mm/yr) is in reddish colors. Precipitations on river headwaters are ≥200 mm/yr to the North and decrease to less than 50 mm/yr southward. (c) Cartoon of the threshold area illustrating tectonic and geomorphic processes: uniform recent uplift of the coastal Andean piedmont driven by recent faulting along the Coastal Scarp (CS), formation of endoreic drainage where rainfall is low and of canyons grading to the ocean where it is higher. AP, WC, WAT, AtP, are Western Cordillera, Altiplano, West Andean Thrust, Atacama Pediplain, respectively. (For interpretation of the references to color in this figure legend, the reader is referred to the web version of this article.)

than 100 km, the drainage system changes from clearly exoreic (northernmost Chile, 18°30′S) to clearly endoreic South of 19°35′S (e.g., Hoke et al., 2007; García et al., 2011) (Figs. 1 and 2). First, we review the geology and geomorphology of the threshold area. Then, we identify and characterize key measurable elements of the landscape. We note that current meteorological data (Strecker et al., 2007; Bookhagen and Strecker, 2008) indicate that the latitudinal rainfall gradient, which is imposed by the modern monsoon, crosses obliquely the Altiplano (AP) and the Western Cordillera (WC) (Fig. 1b) and appears to control spatial variations of drainage erosion power in the threshold area. Finally, using a numerical modeling, we explore a set of scenarios adopting two simple conditions: (1) the topographic relief in the threshold area has experienced uniform tectonic uplift during the past 10 Ma, and (2) the actualistic hypothesis that the present-day pattern of the monsoon regime can help us to explain the long-term development of drainage in the threshold area.

## 2. Geologic, geomorphic and climatic framework

### 2.1. Basic geology and geomorphology

The flat surface of the Pampa del Tamarugal corresponds to the western part of an extensive erosion surface, called Atacama Pediplain (e.g., Hartley and Evenstar, 2010), which marks the top of the continental wedge-shaped Central Depression Basin (CDB), formed between ~30 and ~10 Ma as a foreland basin over the west piedmont of the growing Andes (Hartley and Evenstar, 2010; Schlunegger et al., 2010) (discussing the evolution of the CDB is beyond the scope of this paper however, we present a schematic evolution in Fig. 7). Broad features of the geology of the Andean subduction margin, including the CC, CDB, and Pampa del Tamarugal, follow the geometry of Andean structures, and appear thus controlled by large-scale faults at major boundaries, i.e., the subduction plate contact (Armijo and Thiele, 1990) and the West Andean Thrust (WAT, Fig. 1c; Armijo et al., 2010; Armijo

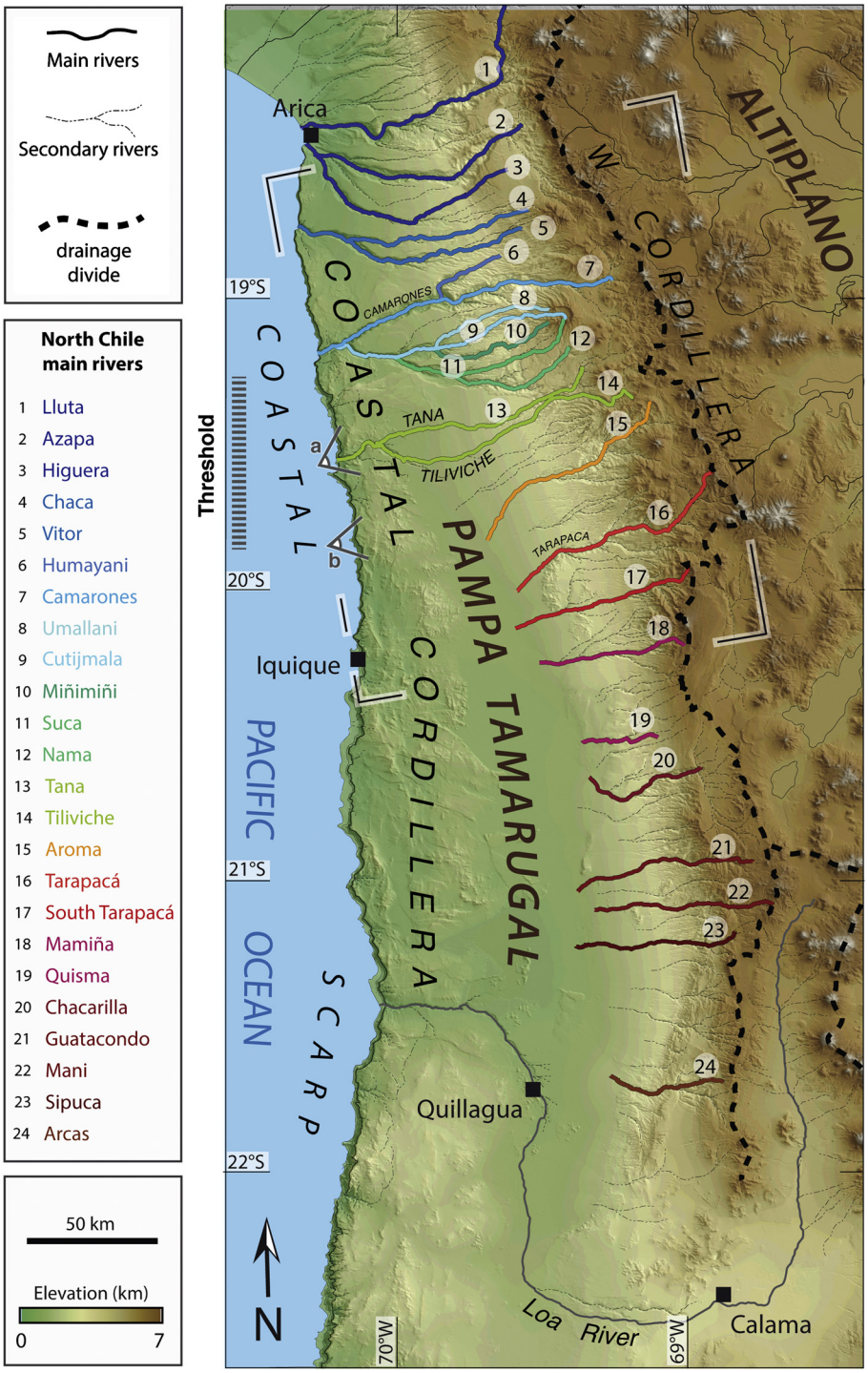


**Fig. 2.** North Chile Topography (SRTM data) and geometry of the drainage network. Profiles of the main river channels, outlined in color, are analyzed in Fig. 3 using the same color code (blue to red) and numbering increasing southward (1 to 24). The heavy dashed line indicates the main drainage divide on top of the Western Cordillera at the western border of the Altiplano. Thin dashed lines mark secondary minor streams (dry most of the time). The threshold between exoreic (to the North) and endoreic (to the South) drainage corresponds to rivers 13 and 14 (Tana–Tiliviche canyons) that present a prominent knick-point at ~25 km to the coast. The only river that crosses the Pampa del Tamarugal and Coastal Cordillera South of the threshold is the Loa river whose catchment area extends far more to the east than the others. View points a and b locate satellite and aerial views shown on Fig. 4. Boxed area corresponds to area covered by the map of Fig. 8a. (For interpretation of the references to color in this figure legend, the reader is referred to the web version of this article.)

et al., in press). In South Peru, the CDB preserves an intercalated marine sediment layer of 25 Ma old (Thouret et al., 2007), which is now found at ~2000 m elevation (Thouret et al., 2007; Schildgen et al., 2009). At that time, sedimentation in the Andes piedmont was occurring close to sea level. Later, the whole sedimentary sequence of the CDB was uplifted and incised by deep canyons grading to the oceanic base level from headwaters located in the WC and AP (Fig. 1). Thermochronology data and $^{40}Ar/^{39}Ar$ age determinations (Thouret et al., 2007; Schildgen et al., 2009, 2010) imply canyon incision after ~9 Ma requiring kilometric differential uplift of the WC with respect to its piedmont and ~1 km of overall land uplift of the whole coastal block (from the coast to the AP) with respect to the oceanic base-level (Schildgen et al., 2009).

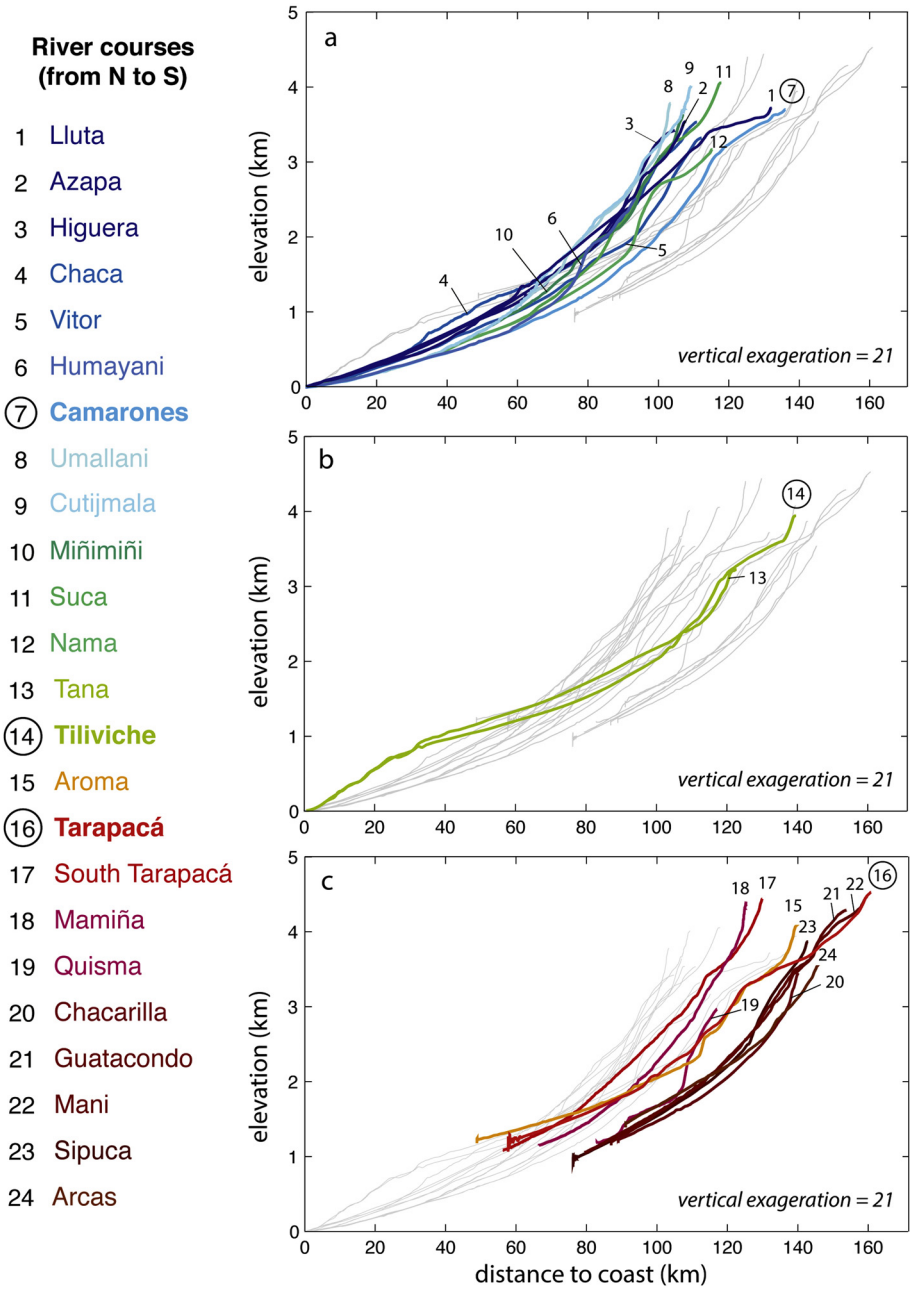


**Fig. 3.** Longitudinal profiles of North Chile main river channels (shown with the same colors as on the map of Fig. 2) extracted from ASTER GDEM data (30 m horizontal resolution and <20 m vertical accuracy). A smoothing with a moving window (window width and overlap: 1 km and 0.4 km) and a wavelet fit are applied to remove spikes and anomalous values. The profiles are separated into three groups: (a) Streams 1 to 12 with an overall concave up shape from high elevations (>4 km a.s.l.) down to sea level; linked to the Pacific Ocean base-level. (b) At the threshold, streams 13 and 14 have a convex upward lower course with a broad knick-point from 0 to ~1 km a.s.l. They remain linked to the ocean base-level. (c) South of the threshold, rivers 15 to 24 vanish in the Pampa del Tamarugal at ~1 km a.s.l. Upper courses of rivers 13 to 24 have an overall concave shape from 4.5 down to 1 km a.s.l., marked by secondary knick-points due to recent uplift of the Western Cordillera (Hoke et al., 2007).

In northernmost Chile, similar canyons have been carved into the whole margin, between the AP and the Pacific. The incision amplitude reaches 1 km deep across the CC and sediments of the CDB. There the top of the CBD corresponds to the Miocene El Diablo formation (Charrier et al., 2007), likely deposited in a braided plain linking the CDB with the Pacific Ocean (Schlunegger et al., 2010) and now found at elevation of ~0.6–1 km close to the coast. The topmost layers of the El Diablo formation are ~8–10 Ma old (Naranjo and Paskoff, 1985; von Rotz et al., 2005; Schlunegger et al., 2010). The maximum onset time of canyon incision is therefore younger than ~10 Ma (García and Hérail, 2005; Schlunegger et al., 2006, 2010; García et al., 2011). This process appears associated with the presence of the 1-km-high Coastal Scarp (Figs. 1, 2, 4; Armijo and Thiele, 1990) as well as with the occurrence of large active normal faulting parallel to that scarp (such as the Pisagua Fault, Fig. 4a). This suggests that, similar to South Peru, significant protracted land uplift relative to the oceanic base level has occurred in North Chile over less than 10 Ma (Armijo and Thiele, 1990; Armijo et al., in press).

### 2.2. Main features of Tiliviche threshold

At 19°35′S, the threshold between exoreic and endoreic drainage (Fig. 2) is accurately defined by using the Tana–Tiliviche river catchment as a reference (Figs. 2, 3b and 4a). The lower course of Tiliviche has a convex upward longitudinal profile and a prominent knick-zone at a distance of ~25 km from the CS (Figs. 3b,

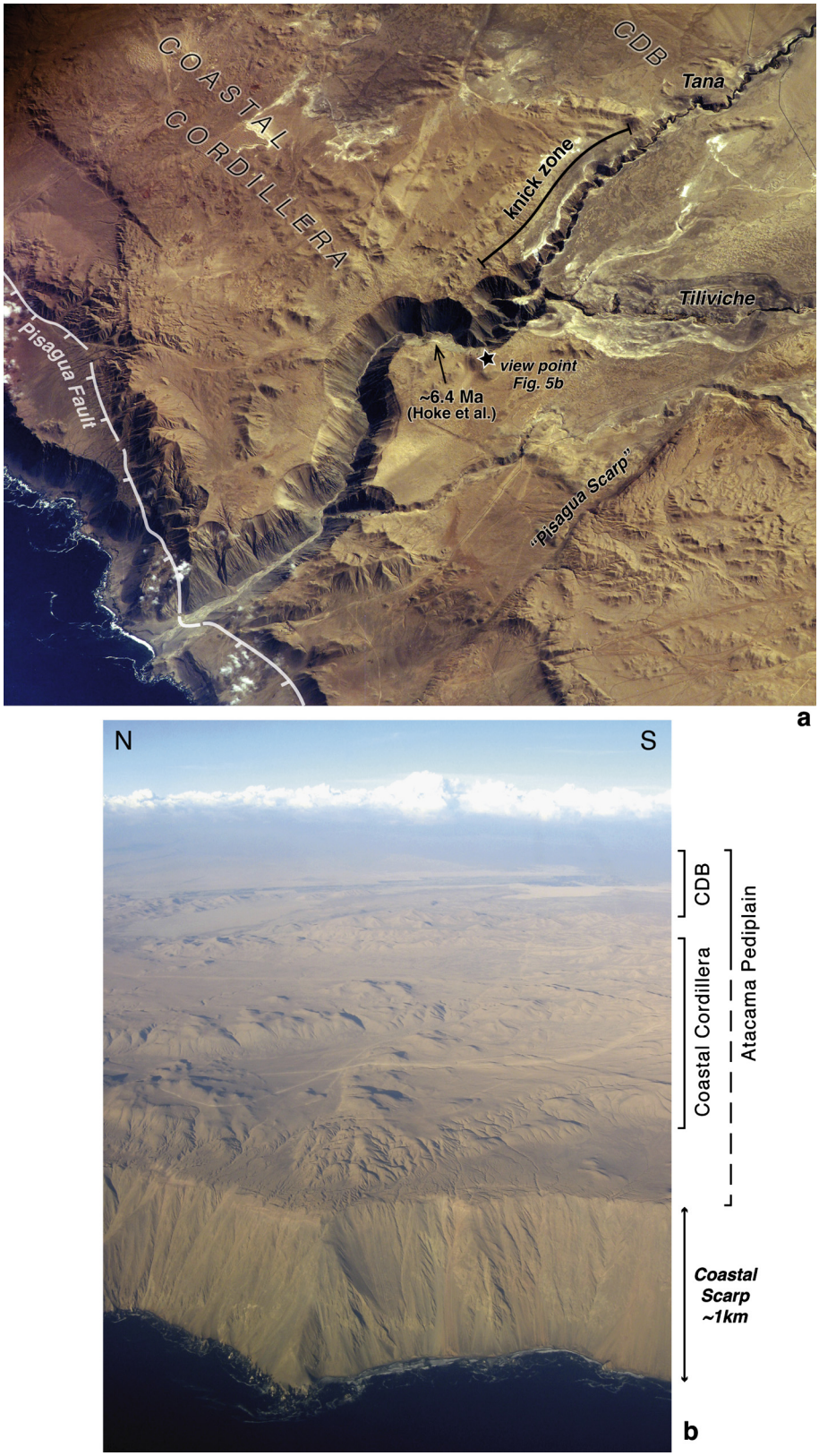


**Fig. 4.** Satellite (a) and aerial (b) views of coastal morphology in the threshold area. (a) Top satellite image (oblique view to NW taken from ISS, courtesy of NASA) shows outlet of Tana–Tiliviche canyon. The tenuously incised Tana upper channel becomes deeply incised downward across the knick zone located at ~25 km from the coast. The normal Pisagua Fault is parallel to the coastal scarp while the minor reverse "Pisagua scarp" (Allmendinger et al., 2005) strikes ENE–WSW. Most of the incision post-date the terrace dated at ~6.4 Ma by Hoke et al. (2007). Note that the surface of the Atacama Pediplain and sediments linked to the Central Depression Basin (CDB) extend on both sides of the canyon up to the Coastal Scarp (where they are offset by the Pisagua Fault), which suggests that the base-level was already set by the ocean before the onset of tectonically-driven uplift and correlative canyon incision. The star locates the viewpoint of panorama from Fig. 5b. (b) Bottom aerial view (courtesy A. Bonacin) shows the impressive Coastal Scarp ~35 km south of Tana–Tiliviche outlet with the Atacama Pediplain and the subdued relief of the Coastal Cordillera perched on top. CDB marks location of the Central Depression Basin in the background.

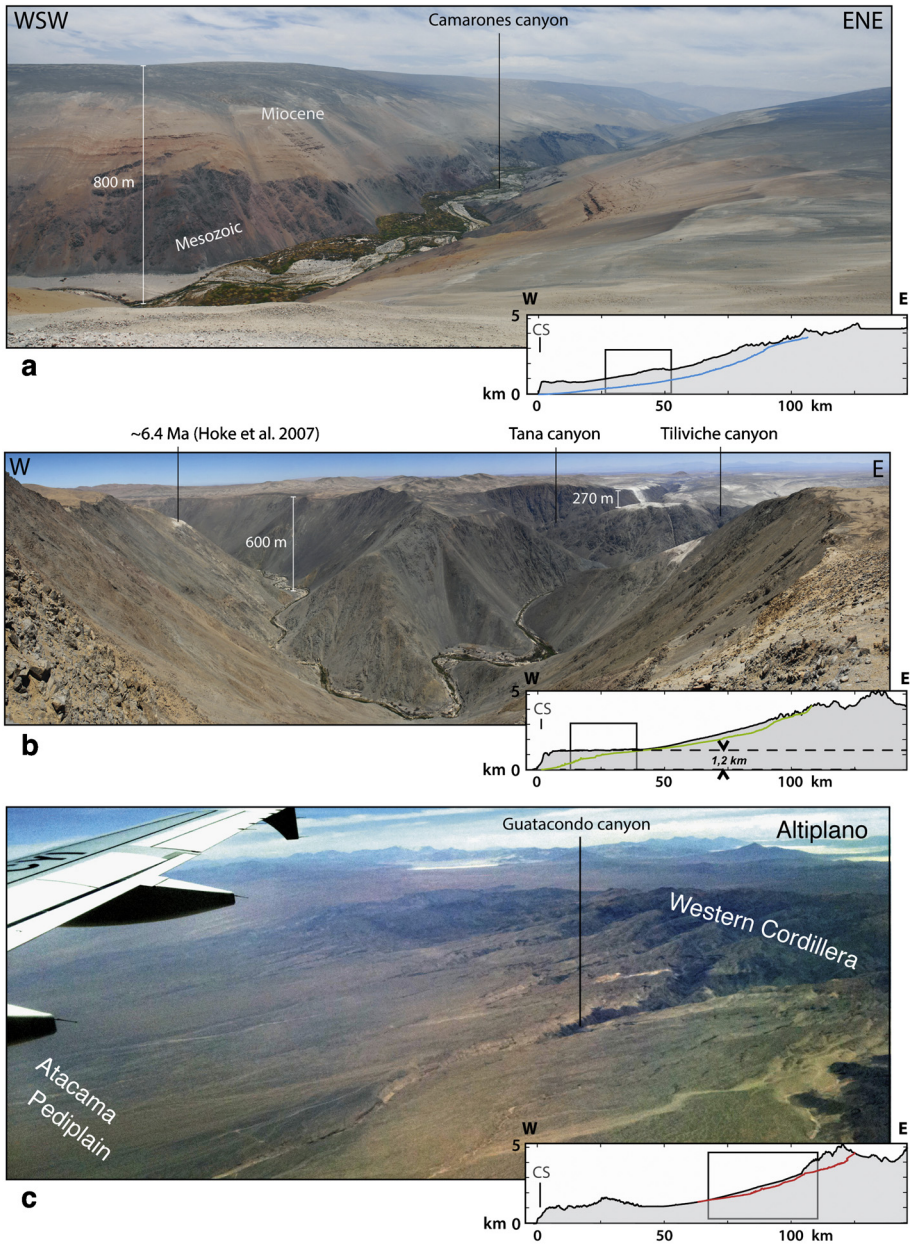


**Fig. 5.** Field views of typical North Chile river morphologies. Lower right insets show the selected river profiles (Camarones, Tiliviche, Tarapacá, Figs. 2, 3, 8) and surrounding topography (box shows part of the profile displayed by the photograph). (a) The Camarones canyon, north of the geomorphic threshold, is incised more than 800 m below the Atacama Pediplain surface within Miocene sediments of the Central Depression Basin and its Mesozoic basement. (b) Panoramic view of the main knick-point characterizing the geomorphic threshold (Tana–Tiliviche canyons). The streams, little incised in the background (right), become deeply entrenched downward into the Mesozoic basement (left). (c) Aerial view (courtesy Y. Lagabrielle) of river channels south of the threshold. The Guatacondo river, in the foreground, which incises the W Cordillera flank and aggrades on the Atacama Pediplain, is similar to the Tarapacá canyon (located more to the North) whose profile is shown on the lower right and on Fig. 8.

4a). There, the stream channel is deeply incised below the Atacama Pediplain surface (≥800 m, Fig. 5b). A dated strath terrace perched at ~50 m below the top of the canyon (Figs. 4a, 5b) located ~15 km from the CS (6.4 Ma, Hoke et al., 2007), suggests that the river was already crossing the CC, reaching the ocean base level before its main incision (Kirk-Lawlor et al., 2013). East of the knick zone (Figs. 4a, 5b), this deep canyon becomes almost superficial (<200 m deep) across the CDB and is limited in its connection with the well-developed upper drainage incising the WC. Rivers to the north of Tiliviche (typified by Camarones, Figs. 2, 5a) are all deeply entrenched from the CS to the WC and show concave longitudinal profiles (Figs. 3a, 5a) for distances of ≥50 km from the CS. South of Tiliviche, the upper rivers incising the WC discharge and aggrade in the Pampa del Tamarugal at ~1 km a.s.l., while a few minor streams drain across the CS to the Pacific (Figs. 2, 3c, 5c). Profiles of those upper drainages reveal several knick-points (Fig. 3c), which are considered to result from differential uplift of the WC relative to the Pampa del Tamarugal surface (Hoke et al., 2007). The only exception to endoreism between 19°35′S and 23°S concerns the Loa river (Fig. 2). Its source is located behind the WC topographic relief, on the Altiplano plateau, with a catchment area much larger than those of endoreic rivers, implying larger water supply and therefore a more efficient erosional power. For further discussion and modeling purposes, we select the three stream profiles typifying the threshold: Camarones, Tiliviche and Tarapacá (Figs. 3 and 5).

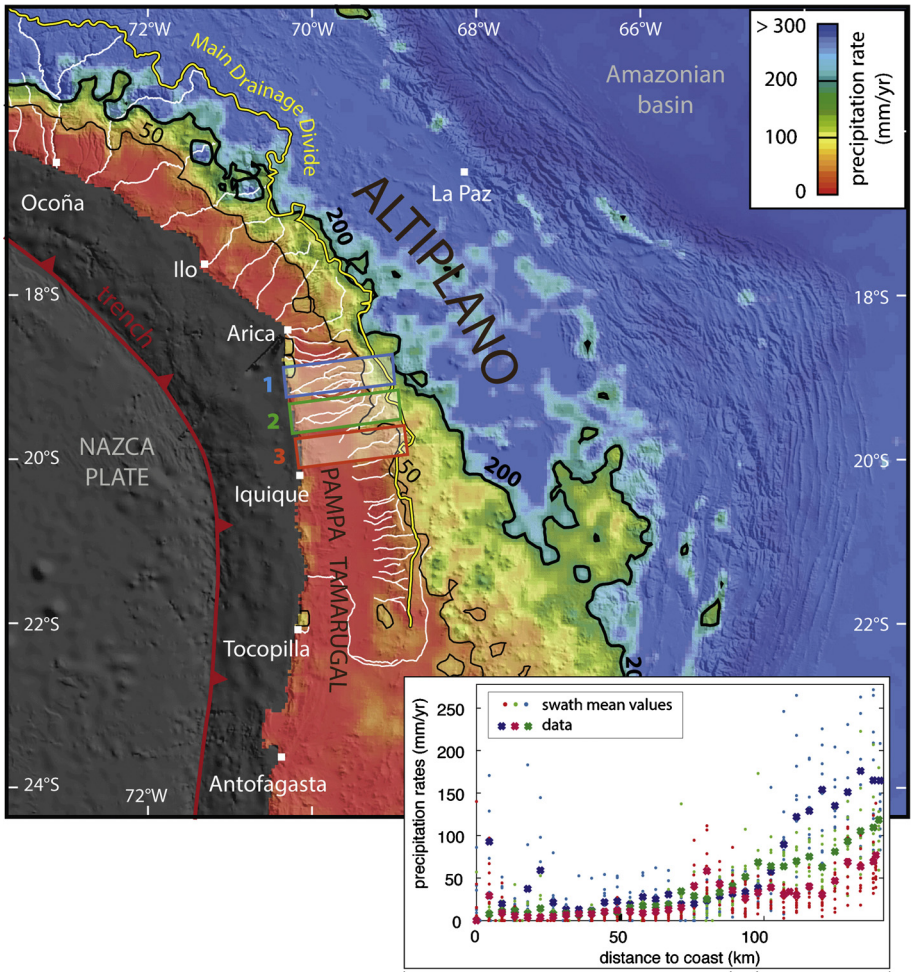


**Fig. 6.** Present-day climatic pattern of the southern Central Andes. Rainfall data (mean annual precipitation rates) come from the TRMM 2B31 dataset (Bookhagen and Strecker, 2008), covering a 9-years long period (1998–2006) and calibrated from field measurements at rain gauge stations. TRMM (Tropical Rainfall Measurement Mission, joint mission of NASA and JAXA) data are available from http://trmm.gsfc.nasa.gov/ and TRMM 2B31 dataset from B. Bookhagen web page: http://www.geog.ucsb.edu/~bodo/TRMM/index.php. We applied a smoothing to original data (0.04° horizontal resolution) using a $5 * 5$ pixel kernel. The color scale is chosen to enhance visualization of driest areas (less than 300 mm/yr). Thin and heavy black lines indicate the 50 mm/yr and 200 mm/yr isohyets, respectively. These isohyets are oblique to the topography of the Altiplano plateau. River (in white) catchment areas reach the 200 mm/yr curve to the NW and become restricted southward below the 50 mm/yr isohyet (except for the Loa river). Boxes numbered 1 to 3 correspond to the three swath profiles shown on the graph below: blue (box 1, North of threshold), green (box 2, threshold) and red (box 3, South of threshold). (For interpretation of the references to color in this figure legend, the reader is referred to the web version of this article.)

For several tens of km North and South of the Tiliviche canyon, the CC is a smooth, relictual relief, which evolved for a long time under extremely low erosion rates (Kober et al., 2007), and have little elevation difference relative to the Pampa del Tamarugal surface (Fig. 4). That low-energy relief is now dramatically rejuvenated by the 1-km-high CS and deep canyon incisions (Figs. 4, 5). We note that the Atacama Pediplain and the CS keep uniform morphology and elevation throughout the threshold area and that all streams are now incised across the same morphologic and geological units (CC, CDB) trending roughly North–South. We infer therefore that differences of stream morphology are not associated with latitudinal variations of uplift rate or of rock erodibility, but more likely to latitudinal variation of river erosional power, which we select as a critical factor for modeling.

### 2.3. *Oblique rainfall gradient over the South Central Andes: hyper-aridity of the Atacama region*

Erosion, and by extension precipitation rates, in the Atacama Desert significantly declined after 15 Ma (e.g., Alpers and Brimhall, 1988; Sillitoe and McKee, 1996), which corresponds to a major global cooling event (see discussion by Gregory-Wodzicki, 2000) and correlates stratigraphically with the end of significant sediment deposition in the CDB and with completion of the Atacama Pediplain. Together with other evidence of long-lived aridity in the Atacama Desert (Houston and Hartley, 2003; Dunai et al., 2005; Hartley et al., 2005; Evenstar et al., 2009) this implies a relatively uniform evolution towards hyper-aridity, clearly established since ~15 Ma.

In the present day, moisture is mostly brought toward the WC and Atacama Desert by northeasterly monsoonal airflow (Houston and Hartley, 2003; Strecker et al., 2007; Garreaud, 2009). The considerable distance from both Atlantic and Amazonian sources of humidity to the western Andean margin is the first cause of hyper-aridity in the Atacama. Other factors, such as the cold Humboldt oceanic current, also contribute to hyperaridity by preventing inland penetration of moisture coming from the Pacific (Houston and Hartley, 2003; Garreaud, 2009). As a consequence, present-day precipitation decreases southwestward across the AP, causing isohyets to be oblique to the Andean relief south of 15°S (Houston and Hartley, 2003; Bookhagen and Strecker, 2008; Garreaud, 2009) and producing the latitudinal rainfall gradient over the western AP and WC clearly visible in maps (Figs. 1, 6). In South Peru, the gradient is parallel to the coast and the WC

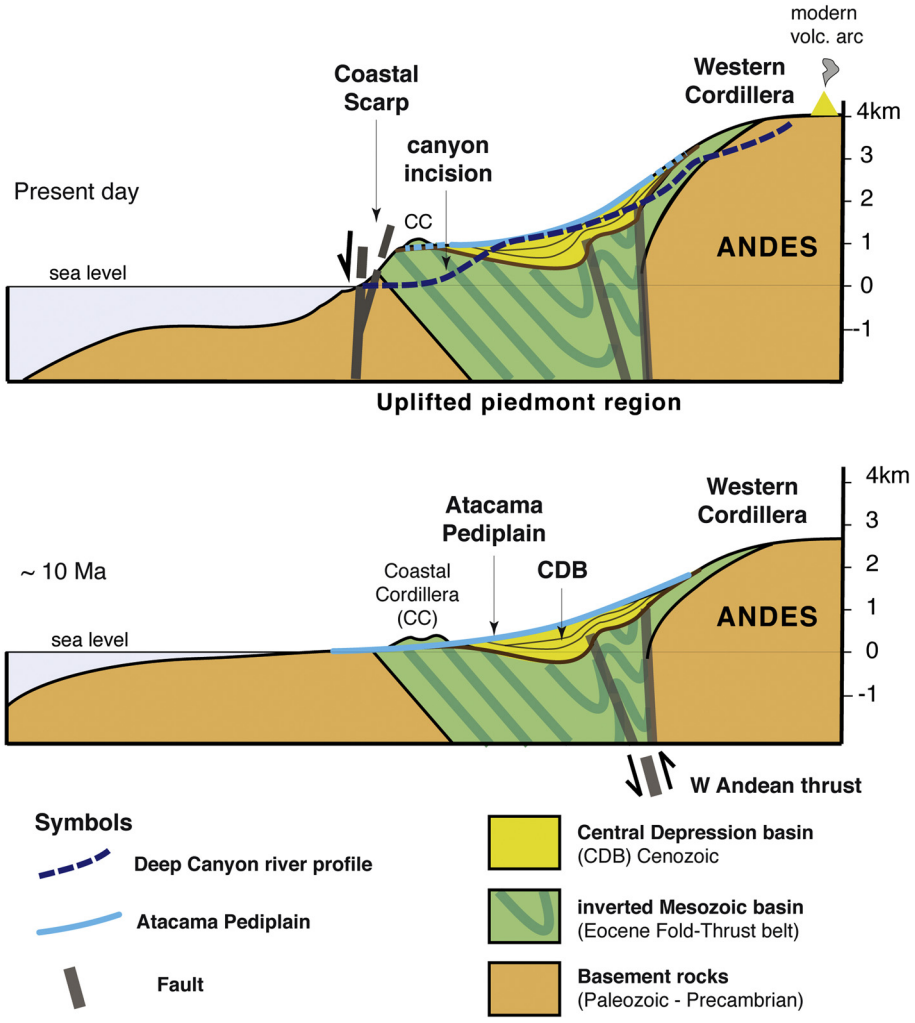


**Fig. 7.** Schematic morpho-tectonic evolution of the west Andean margin for the last 10 Myr. (Top) Present-day topography and geology of the coastal topography. The Atacama Pediplain (AtP) is hanging at 1 km a.s.l. and is interrupted towards the coast by the giant Coastal Scarp. The AtP corresponds to the top surface of a continental wedge-shaped basin: the Central Depression Basin, which is deeply incised by rivers all the way from the Western Cordillera to the ocean. (Bottom) Possible reconstruction of the 10 Ma topography of the west Andean margin. The Atacama Pediplain is a smooth and continuous surface that connects with the ocean base level.

and headwaters of catchments draining to the Pacific experience precipitation rates $\geq$200 mm/yr (Fig. 6). In North Chile, mean annual rainfall on the WC decreases southward to $\leq$50 mm/yr south of $\sim$20°S (Fig. 6). In both South Peru and North Chile, rainfall is almost null on the Pampa del Tamarugal and towards the coast ($\leq$5 mm/yr of precipitation). Regarding our actualistic modeling approach, we retain the observed oblique spatial pattern of present-day rainfall in the WC, upstream from the three catchments typifying the Tiliviche threshold. In other words, our approach assumes and tests stability over the long term of oblique monsoonal conditions across the WC, which is consistent with long-lived hyper-aridity in the Atacama Desert and with evidence for monsoonal conditions in the eastern Andes, on the landward side of the Altiplano, since $\sim\geq$10 Ma (Uba et al., 2007; Mulch et al., 2010).

### 2.4. North Chile canyon incision: climatic or tectonic driver?

In contrast with the evidence summarized above and the doubtless recent uplift of coastal South Peru (Schildgen et al., 2007, 2009), it has for long been considered that uplift of coastal regions in North Chile would be much older than the $\sim$<10 Ma incision of canyons (e.g., Mortimer and Saric, 1975; Farías et al., 2005; García et al., 2011). It has been suggested that the top surface of the CDB was dammed by pre-existing CC reliefs and stood for a long time as an elevated base level not connected to the ocean (e.g., Mortimer and Saric, 1975; García et al., 2011). Canyon incision, and eventual connection of the drainage to the ocean, would have been recently triggered by runoff increases associated with hypothetic semi-arid pulses interrupting the prevalent hyper-arid regime (García et al., 2011). This transition to exoreic drainage would have been more efficient and rapid in the North because of the latitudinal rainfall gradient (García et al., 2011). These authors also consider that incision processes would not have been synchronous along the margin. There is no compelling geological evidence for such a complex scenario and the notion of old uplift ($\sim\geq$25 Ma) with uncorrelated incision appears controversial (e.g. Zeilinger et al., 2005; Kober et al., 2006; Schildgen et al., 2007; Schlunegger et al., 2006, 2010; Hoke et al., 2007; Jordan et al., 2010; Kirk-Lawlor et al., 2013). So here, we choose to retain the simplest hypothesis of relatively stable hyper-aridity since $\sim$15 Ma, and to test the idea that the flat, western part of the Atacama Pediplain was initially forming an Andean piedmont close to the ocean base-level (Fig. 7), and that overall uplift of this piedmont relative to the ocean triggered the headwards incision of canyons since $\sim$<10 Ma (García and Hérail, 2005; Schildgen et al., 2007; Schlunegger et al., 2006, 2010; Kirk-Lawlor et al., 2013).

## 3. Modeling of drainage evolution

### 3.1. Modeling strategy

From the descriptions and discussion detailed in Section 2, we retain several relevant statements for our modeling of drainage in North Chile: (1) the uplift of the Andean piedmont starts at ~10 Ma or even younger and triggered headwards incision of rivers (Fig. 7) as demonstrated for canyons in South Peru; (2) the first-order geomorphic and geological continuity of coastal units throughout the identified drainage threshold implies that differences of stream morphology are likely associated with latitudinal variation of river erosional power; (3) the threshold between exoreic and endoreic drainage regimes is correlated with the latitudinal gradient imposed by the modern monsoon (carrying humidity from the Atlantic); (4) the hyper-aridity on coastal North Chile and the present-day oblique monsoonal conditions across the WC are stable features on the long-term. We use these inferences to settle a numerical model of landscape evolution using the code of Carretier and Lucazeau (2005).

### 3.2. The numerical landscape model APERO

As with other landscape evolution models (e.g. SIBERIA, Willgoose et al., 1991, CAESAR, Coulthard et al., 2002, GOLEM, Tucker and Slingerland, 1994, CASCADE, Braun and Sambridge, 1997, CHILD, Tucker and Bras, 2000, EROS, Davy and Crave, 2000), the APERO code models landscape evolution by routing water and sediments over a grid of regular cells, starting from cells at the highest elevation and moving progressively to the lowest ones. It calculates elevation changes according to sediment production resulting from diffusion, alluvial transport and bedrock incision. The principles of APERO (Carretier and Lucazeau, 2005) are described here in simple terms and in more detail in the Supplementary Information.

The governing equations used in APERO are the conservation equations of mass for water (1) and for sediments (2) that are separately numerically solved with the finite difference method.

$$\frac{\partial h_f}{\partial t} - Q_{f\,\mathrm{IN}} + Q_{f\,\mathrm{OUT}} = 0 \tag{1}$$

with $h_f$ the water thickness integrated over the cell size, $Q_{f\,\mathrm{IN}}$ the input water flux and $Q_{f\,\mathrm{OUT}}$ the output water flux.

$$\frac{\partial h_s}{\partial t} - Q_{s\,\mathrm{IN}} + Q_{s\,\mathrm{OUT}} + U = 0 \tag{2}$$

with $h_s$ the ground elevation integrated over the cell size, $Q_{s\,\mathrm{IN}}$ the input sediment flux, $Q_{s\,\mathrm{OUT}}$ the output sediment flux and $U$ the tectonic uplift rate integrated over the cell size. In (1) and (2), the fluxes and the uplift rate have dimensions of $[L^3T^{-1}]$.

$Q_{f\,\mathrm{IN}}$ scales with the effective mean precipitation rate within the catchment relative to the cell $(i)$, including the cell $(i)$ itself.

$$Q_{f\,\mathrm{IN}(i)} = \int_A P_d(x, y)\,\mathrm{d}s \tag{3}$$

$P_d$ is the effective mean precipitation rate $[LT^{-1}]$ and $A$ is the catchment area relative to cell $i$.

Each cell $(i)$ interacts with its neighboring cells $(j)$ depending on the difference in topography between the two cells. We define $S_{ij} = \max(0, (h_i - h_j)/d_{ij})$ where $d_{ij}$ is the distance between the two cells. The distribution of water from cell $i$ to cell $j$ $(Q_{f\,\mathrm{OUT}(ij)})$ follows (4), called multiple flow algorithm:

$$Q_{f\,\mathrm{OUT}(ij)} = Q_{f\,\mathrm{IN}(i)} \frac{S_{ij}}{\sum_j S_{ij}} \tag{4}$$

The total output flux $Q_{f\,\mathrm{OUT}(i)}$ is the sum over $(j)$ of the local $Q_{f\,\mathrm{OUT}(ij)}$.

The input sediment flux $Q_{s\,\mathrm{IN}(i)}$ on a cell $i$ is the sum of the local outputs $Q_{s\,\mathrm{OUT}(ij)}$ of sediments from the upper cells which are distributed according to the following algorithm.

The output sediment flux $Q_{s\,\mathrm{OUT}(i)}$ on a cell $(i)$ (5) corresponds to the joint action of diffusion processes (6) and (7), alluvial transport (8) and bedrock incision processes (9) occurring on a cell,

$$Q_{s\,\mathrm{OUT}} = Q_{\mathrm{snldiff}} + Q_{\mathrm{sal}} + Q_{\mathrm{br}} \tag{5}$$

The component of sediment output due to bedrock diffusion processes, $Q_{\mathrm{snldiff}}$ or diffusive transport rate (6), is written as a non-linear diffusion equation (Roering et al., 1999) (7) to take into account landslide processes where:

$$Q_{\mathrm{snldiff}} = \nabla . q_{\mathrm{snldiff}} \tag{6}$$

$$q_{\mathrm{snldiff}} = -\kappa \frac{\nabla h_s}{1 - (\frac{\nabla h_s}{S_c})^2} \tag{7}$$

with $S_c$ the critical slope corresponding to the gradient of repose of sediments or bedrock and $\kappa$ a diffusion coefficient $[L^2T^{-1}]$. Note that $\kappa$ depends on rock type (either sediment, or bedrock or a combination of the two, see Supplementary Information).

The alluvial transport flux, $Q_{\mathrm{sal}}$, and the bedrock incision flux integrated over the river width, $Q_{\mathrm{br}}$, are written as power-law equations:

$$Q_{\mathrm{sal}} = K_{\mathrm{al}} Q_{f\,\mathrm{OUT}}^{\alpha} S_{ij}^{\beta} \tag{8}$$

$$Q_{\mathrm{br}} = K_{\mathrm{br}} Q_{f\,\mathrm{OUT}}^{m} S_{ij}^{n} \tag{9}$$

where $K_{\mathrm{al}}$ and $K_{\mathrm{br}}$ are positive coefficients with dimensions $[L^{3-3\alpha}T^{\alpha-1}]$ and $[L^{3-3m}T^{m-1}]$. $\alpha$, $\beta$, $m$ and $n$ determine the degree of non-linearity of the two laws and $m$ and $n$ have values comprised between 0 and 2 (Stock and Montgomery, 1999).

Further details on the numerical implementation and on model calibration (grid size, characterization of $K_{\mathrm{al}}$, $\alpha$, $\beta$, $K_{\mathrm{br}}$, $m$ and $n$, choice of parameters values, etc.) are given in the Supplementary Information (SI) with pertinent references herein.

### 3.3. Model setting

We ran numerical experiments of landscape evolution using the modeling code of Carretier and Lucazeau (2005). The experimental grid is scaled to reproduce the topography of the threshold area of North Chile and to reach the present-day stage after 7 Myr of evolution: the minimum likely age for North Chile onset time of incision. Experiments start with an initially flat, low-energy coastal topography that lies at sea level. The WC–AP is a pre-existing relief (Victor et al., 2004; Hoke et al., 2007; Jordan et al., 2010). In agreement with the geological constraints, a value of 0.14 mm/yr is used for the uplift rate at the coast rising to 0.22 mm/yr at the WC (see Supplementary Information for a detailed discussion). Those rates remain constant during the experiment. The final modeled topography compares well with the current one, including the formation of a 1-km-high CS (Fig. 7, Fig. S1). Rainfall is null at the coast and on the Pampa del Tamarugal surface and is mostly localized above the upper WC and AP reliefs (Fig. S1). Several values of precipitation rates were tested (from 20 to 200 mm/yr on the WC) to take into account the possible effect of the latitudinal rainfall gradient. Infiltration and evaporation cannot be addressed by our modeling, so water flows at the surface and goes out from the model grid at its left (West) boundary (Carretier and Lucazeau, 2005). Refer to Supplementary Information (SI) (Table S1 and Figs. S2 to S9) for a complete summary of other boundary conditions. Parameters controlling the physics of the erosion processes are fixed according to published values

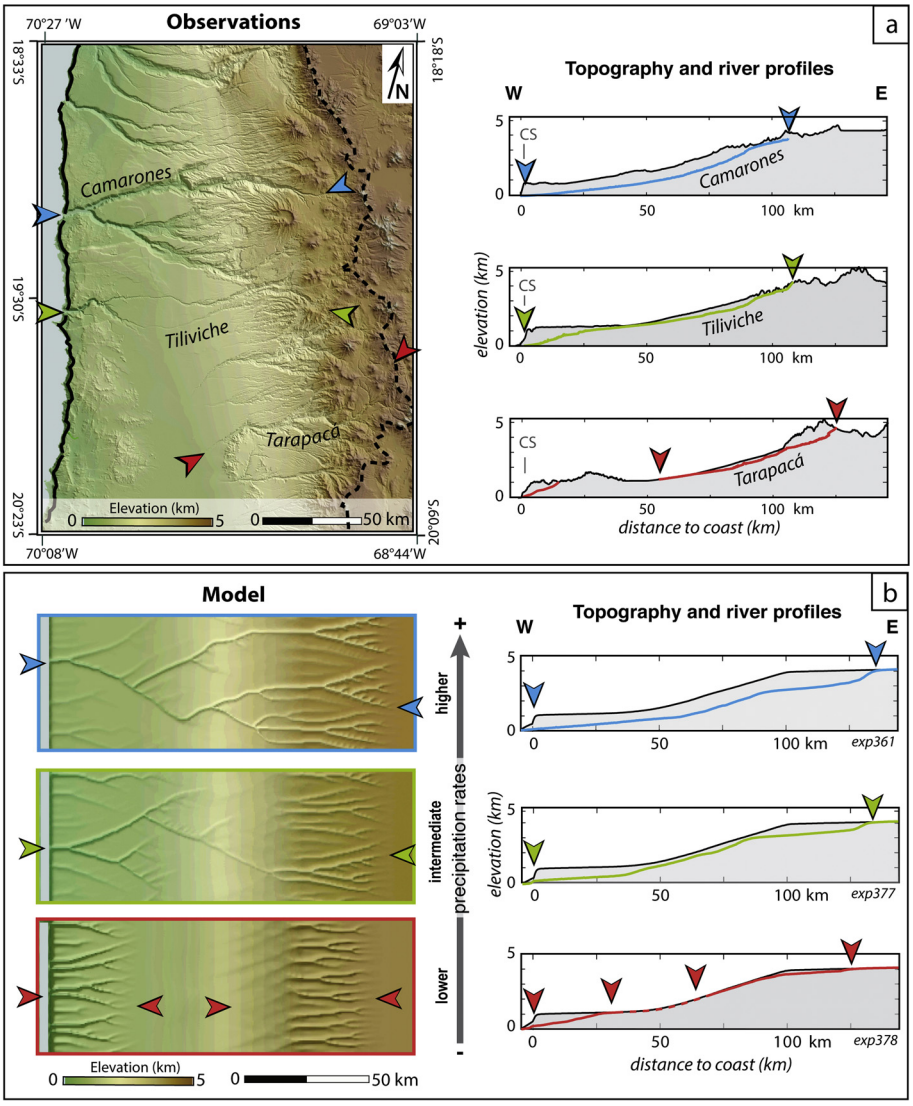


**Fig. 8.** Geomorphology of the threshold area (see location on Figs. 1 and 2). (a) Map view (left) displays the three channels selected to illustrate the threshold between exoreic and endoreic drainage. On the right: longitudinal river profiles (projected E–W) and surrounding topographic envelope for these three typical valleys: Camarones (North of threshold, linked to ocean base-level and deeply entrenched), Tiliviche (threshold, convex upward and with prominent knick-point), Tarapacá (South of threshold, endoreic). (b) Selected modeling results (map views) for three different mean precipitation rates (see Fig. S5 for a view of the whole experimental boxes). Same initial topography and uplift rates are used for all the experiments. On the right, representative topography and river profiles, drawn for the streams outlined by arrows on map views to the left, to be compared with Camarones, Tiliviche and Tarapacá river profiles.

(references given in SI), or chosen among values producing the observed morphology, after sensitivity analyses (see SI Part C, Table S2 and Figs. S2 to S9).

## 4. Experimental modeling results, limitations and implication

### *4.1. Topography and river drainage evolution: model vs. natural landscape*

We simulate the evolution of river incision onto an uplifting coastal block under three different constant rainfall conditions (low, intermediate and high precipitation rates) during 7 Myr in agreement with the present-day precipitation rates (PR) distribution over North Chile. Fig. 8b shows the modeling results of the three corresponding experiments where river long profiles can be compared to the three stream profiles typifying the threshold in North Chile: Camarones, Tiliviche and Tarapacá. In the experiments, dendritic drainage catchments form as the coastal topography rises without being significantly eroded, except where river incision develops.

For the higher values of PR (Fig. 8b-top), the main streams are deeply incised in the coastal topography and grade to the oceanic base level. The river profile is nearly in equilibrium for ~80 km from the coast up to the WC. This result is comparable to the Camarones river profile that is uniformly deeply entrenched in the topography from the Altiplano plateau towards the oceanic base level. Water supply appears therefore to be sufficient to allow a full river incision from high elevations (4000 m) to the oceanic base level.

For the intermediate PR values (Fig. 8b-middle), the stream presents a concave shape; lower and upper stream courses are nearly separated, with little incision in the middle course, and a knick-point forms at ~40 km from the coast. This concave shape means that the stream is not in equilibrium, contrary to the first experiment with higher value of PR. The profile is comparable to the Tiliviche river profile whose incision is five times lower in the middle of the coastal plateau than it is closer to the Coastal Scarp. This implies that water supply is not high enough to enable a spatially constant incision into the uplifting topography.

For the lower PR values (Fig. 8b-bottom), incision in the middle course of streams is replaced by aggradation on top of the rising coastal topography. The water flows at the surface and drives incision of the lower course and formation of a knick-point at ~20 km from the coast. This numerical experiment result can be compared to the Tarapacá river incision. The stream incises only the upper part of the topography, does not entrench the coastal plateau and consequently does not reach the oceanic base level.

### 4.2. Limitations and drawbacks

We acknowledge that our experiments are simple first-order ones and do not take into account several natural processes occurring in North Chile that may play a role on the final results. However, we note that our results compare qualitatively well with the observed landscape morphology and its variability. Yet, our modeling approach has some limitations that we discuss here before further exploring the implications of the results.

First, the model involves 12 parameters for most of which there is no direct natural geological or hydrological quantitative constraints. So, it has been necessary to (1) determine the dominant parameter for our modeling and investigate the effects of its possible values and (2) calibrate each parameter with tests within ranges of published values. Because there is little sediment cover on the riverbed in North Chile, the evolution of topography is likely governed by detachment-limited process justifying the choice of the bedrock incision parameter ($K_{br}$) as one of the main controls in our modeling. As there is no specific constraint for this parameter respective to North Chile rivers, we tested several values published in the literature and considered two end-members values along with an intermediate one. We ran a sensitivity analysis for each of the other parameters and calibrated the model with their most pertinent value (cf. SI). We present here our preferred solution and we acknowledge that this is not a unique solution.

Second, while most authors regroup rock erodibility and climatic effects into the bedrock incision parameter, an assumption that is correct for steady-state systems, we note that, in a transitory regime, PR also acts in the alluvial transport process (8). This justifies our choice to use distinct $K_{br}$ and PR. Our results imply that, for a given value of $K_{br}$, the threshold between exoreic and endoreic drainage systems is controlled by differences in PR. However, comparable result could have been obtained for other combinations of $K_{br}$ and PR. Increasing erodibility balances with decreasing PR, and inversely (9). Our sensitivity analysis highlights this trade-off between erodibility and PR (see Figs. S5 to S9).

Third, we use mean annual PR values derived from present day precipitation rates measured over a 9 yr period (1998 to 2006) (data from Bookhagen and Strecker, 2008). Extrapolating those present-day rates over a 7 Myr-time scale is justified by studies of erosion, mineralization and soil development carried out in the Atacama Desert that show that PR have been lower than 200 mm/yr over the last 20 Myr (Alpers and Brimhall, 1988; Rech et al., 2006). However, rainfall in the Atacama Desert area occurs as infrequent distinct events of relatively large amplitude and not as continuous rainfall. Bedrock incision due to such discrete events is likely higher than the incision resulting from a constant mean rainfall. We used a 10-yr time step in the modeling that simulates to a certain degree this kind of discrete rainfall event. However, the influence of short-term (10–100 yr) variability of PR on the evolution of the landscape will have to be more carefully investigated for further quantitative studies.

Other limitations come from the fact that our modeling does not allow for evaporation of infiltration. In North Chile (Fig. 8a middle and bottom), part of the water flow leaks or evaporates while crossing the Pampa del Tamarugal, resulting in less incised lower streams than in the experiments, and knick-points closer to the coast. Another difference is that the experimental upper course of catchments is also more entrenched into the WC topographic relief than in nature (compare natural and experimental river profiles on Fig. 8). It is probable that part of the precipitation occurring over the west AP and WC does not contribute to the surface flow and instead infiltrates the bedrock causing springs to form at lower elevation on the flanks of the WC as described by Hoke et al. (2004). Also, thick resistant flows of Miocene ignimbrite cover the WC topography and may prevent efficient erosion. In our experiments, we used a uniform bedrock incision parameter over the entire box, but the effect of this ignimbritic cover may be assessed looking at the sensitivity analyses for different values of $K_{br}$.

Time scaling is difficult to test with our experiments. We must acknowledge that we adjusted the modeling parameter values to allow for drainage development over a 7 Myr-time scale, which is deduced from geological observations for the onset of incision (e.g. Naranjo and Paskoff, 1985; Hoke et al., 2004). With this taken into account, we note that with constant uplift rate and different values for PR, our model, run for 7 Myr, is able to reproduce the different drainage systems we identified in the threshold area.

### 4.3. Climatic and geodynamic implications

From the comparison of experimental and natural drainages (Fig. 8), we deduce that retaining experimental PR values in the range of present-day values is enough to explain the development of that drainage, including its latitudinal variation and specifically the occurrence of the Tiliviche threshold. More specifically, under constant tectonic uplift, the occurrence of that threshold requires a stable latitudinal gradient of precipitation over the WC, similar to the modern one. We note that the condition of keeping such stable latitudinal PR gradient needs to take into the account the trade-offs between the different modeling parameters and in particular the one between basement erodibility and precipitation rate. This implies a set of possible stable solutions consistent with monsoon regimes with different precipitation intensity (within a range of PR values), but maintaining stable spatial extent and latitudinal gradient over the WC.

Both geological observations and model support the idea of a flat low-energy coastal morphology located close to the Pacific Ocean base level as initial conditions prior to ca. 7 Ma. As there may be a lag time between uplift and related incision processes, we consider the age of 7 Ma as a minimum age for the onset of uplift, which could be a few millions years older. So, at ~10 Ma, in North Chile and South Peru, the southwestern Andean piedmont had probably begun to experience synchronous and uniform uplift triggered by a dramatic tectonic change. The uplift added ~1 km of elevation to the onshore Andean subduction margin limited to the West by the Coastal Scarp (Fig. 1c). This recent uplift of the coastal topography implies to consider a trench-ward enlargement of the Andean topographic relief by incorporation of the coastal Atacama region to the Andes–Altiplano orogen (Armijo et al., in press). Deep crustal underplating, probably associated with fault geometrical complexities at the subduction plate interface and above (Armijo and Thiele, 1990; Contreras-Reyes et al., 2012), is a possible cause of coastal uplift and widening of the Andean orogen (Armijo et al., in press). Structural complexities may also control segmentation of the mechanically coupled zone at the subduction interface, as recently suggested by Béjar-Pizarro et al. (2013). So, recent (<10 Ma) Andean deformation is not only located on the eastern side of the orogen as generally admitted (e.g. McQuarrie, 2002; Oncken et al., 2006) but also proceeds by widening of the belt towards the subduction, which brings new insights into the process of propagation of the deformation across the entire mountain range.

## 5. Conclusions

Numerical modeling of landscape evolution in North Chile allowed us to test the hypothesis of recent uniform tectonic uplift driving river incision in the past 10 Myr over the west Andean margin. Our results offer a simple framework with a reduced number of semi-quantitative geomorphic parameters, which we used to explain the modern evolution of both, morphology and tectonics, as deciphered from their quantitative imprint in the present-day landscape. An important result is that the latitudinal transition from exoreic to endoreic drainage systems across the Atacama Desert of North Chile would be primarily controlled by a spatial gradient of precipitation rates over the headwaters of rivers in the Western Cordillera. Gradient patterns required in our modeling are similar to present-day conditions of precipitation rates; a result suggesting that the rainfall patterns in the Western Cordillera and the Atacama Desert, largely controlled by the effect of Atlantic monsoon, are long-lived features of Andean climate.

## Acknowledgements

Work supported by an IPGP-Univ. Paris Diderot PhD grant to A. Coudurier-Curveur and funded by CNRS-INSU (SYSTER program, project "Diachronisme du West Andean Thrust"), ANR project MegaChile (grant ANR-12-BS06-0004-02), and the LABEX UnivEarthS (Sorbonne Paris Cité, Work Package 1). We benefited from fruitful discussions with D. Carrizo in the field and with F. Métivier on the experimental approach. We thank anonymous reviewers and the editor for their very helpful and constructive comments.

## Appendix A. Supplementary material

Supplementary material related to this article can be found online at http://dx.doi.org/10.1016/j.epsl.2014.12.047.

## References

Allmendinger, R.W., González, G., Yu, J., Hoke, G., Isacks, B., 2005. Trench-parallel shortening in the Northern Chilean Forearc: tectonic and climatic implications. Geol. Soc. Am. Bull. 117 (1), 89. http://dx.doi.org/10.1130/B25505.1.

Alpers, C.N., Brimhall, G.H., 1988. Middle Miocene climatic-change in the Atacama Desert, northern Chile – evidence from supergene mineralization at La Escondida. Geol. Soc. Am. Bull. 100 (10), 1640–1656. http://dx.doi.org/10.1130/0016-7606(1988)100<1640:mmccit>2.3.co;2.

Armijo, R., Thiele, R., 1990. Active faulting in northern Chile: ramp stacking and lateral decoupling along a subduction plate boundary? Earth Planet. Sci. Lett. 98 (1), 40–61. http://dx.doi.org/10.1016/0012-821X(90)90087-E.

Armijo, R., Rauld, R., Thiele, R., Vargas, G., Campos, J., Lacassin, R., Kausel, E., 2010. The West Andean Thrust, the San Ramón Fault, and the seismic hazard for Santiago, Chile. Tectonics 29, TC2007. http://dx.doi.org/10.1029/2008TC002427.

Armijo, R., Lacassin, R., Coudurier-Curveur, A., Carrizo, D., in press. Coupled tectonic evolution of Andean orogeny and global climate. Earth-Sci. Rev.

Béjar-Pizarro, M., Socquet, A., Armijo, R., Carrizo, D., Genrich, J., Simons, M., 2013. Andean structural control on interseismic coupling in the North Chile subduction zone. Nat. Geosci. 6, 462–467. http://dx.doi.org/10.1038/NGEO1802.

Bonnet, S., Crave, A., 2003. Landscape response to climate change: insights from experimental modeling and implications for tectonic versus climatic uplift of topography. Geology 31 (2), 123–126. http://dx.doi.org/10.1130/0091-7613(2003)031<0123:LRTCCI>2.0.CO;2.

Bookhagen, B., Strecker, M.R., 2008. Orographic barriers, high-resolution TRMM rainfall, and relief variations along the eastern Andes. Geophys. Res. Lett. 35 (6), L06403. http://dx.doi.org/10.1029/2007GL032011.

Braun, J., Sambridge, M., 1997. Modelling landscape evolution on geological time scales: a new method based on irregular spatial discretization. Basin Res. 9, 27–52.

Carretier, S., Lucazeau, F., 2005. How does alluvial sedimentation at range fronts modify the erosional dynamics of mountain catchments? Basin Res. 17, 361–381. http://dx.doi.org/10.1111/j.1365-2117.2005.00270.x.

Charrier, R., Pinto, L., Rodríguez, M.P., 2007. Tectonostatigraphic evolution of the Andean Orogen in Chile. In: Moreno, T., Gibbons, W. (Eds.), The Geology of Chile. The Geological Society, London, pp. 21–114.

Contreras-Reyes, E., Jara, J., Grevemeyer, I., Ruiz, S., Carrizo, D., 2012. Abrupt change in the dip of the subducting plate beneath north Chile. Nat. Geosci. 5, 342–345. http://dx.doi.org/10.1038/ngeo1447.

Coulthard, T.J., Macklin, M.G., Kirkby, M.J., 2002. A cellular model of Holocene upland river basin and alluvial fan evolution. Earth Surf. Process. Landf. 27 (3), 269–288.

Davy, P., Crave, A., 2000. Upscaling local-scale transport processes in large-scale relief dynamics. Phys. Chem. Earth, Part A, Solid Earth Geod. 25 (6–7), 533–541. http://dx.doi.org/10.1016/S1464-1895(00)00082-X.

Dunai, T.J., González López, G.A., Juez-Larré, J., 2005. Oligocene–Miocene age of aridity in the Atacama Desert revealed by exposure dating of erosion-sensitive landforms. Geology 33, 321–324. http://dx.doi.org/10.1130/G21184.1.

Evenstar, L., Hartley, A., Stuart, F., Mather, A., Rice, C., Chong, G., 2009. Multiphase development of the Atacama Planation Surface recorded by cosmogenic $^{3}$He exposure ages: implications for uplift and Cenozoic climate change in western South America. Geology 37, 27–30. http://dx.doi.org/10.1130/G25437A.1.

Farías, M., Charrier, R., Comte, D., Martinod, J., Hérail, G., 2005. Late Cenozoic deformation and uplift of the western flank of the Altiplano: evidence from the depositional, tectonic, and geomorphologic evolution and shallow seismic activity (northern Chile at 19°30′S). Tectonics 24, TC4001. http://dx.doi.org/10.1029/2004TC001667.

García, M., Hérail, G., 2005. Fault-related folding, drainage network evolution and valley incision during the Neogene in the Andean Precordillera of Northern Chile. Geomorphology 65, 279–300.

García, M., Riquelme, R., Farías, M., Hérail, G., Charrier, R., 2011. Late Miocene–Holocene canyon incision in the western Altiplano, northern Chile: tectonic or climatic forcing? J. Geol. Soc. 168, 1047–1060. http://dx.doi.org/10.1144/0016-76492010-134.

Garreaud, R.D., 2009. The Andes climate and weather. Adv. Geosci. 22, 3–11. http://dx.doi.org/10.5194/adgeo-22-3-2009.

Gregory-Wodzicki, K.M., 2000. Uplift history of the Central and Northern Andes: a review. Geol. Soc. Am. Bull. 112 (7), 1091–1105. http://dx.doi.org/10.1130/0016-7606(2000)112<1091:uhotca>2.3.co;2.

Hartley, A.J., Evenstar, L., 2010. Cenozoic stratigraphic development in the north Chilean forearc: implications for basin development and uplift history of the Central Andean margin. Tectonophysics 495, 67–77. http://dx.doi.org/10.1016/j.tecto.2009.05.013.

Hartley, A.J., Chong, G., Houston, J., Mather, A.E., 2005. 150 million years of climatic stability: evidence from the Atacama Desert, northern Chile. J. Geol. Soc. 162 (3), 421–424. http://dx.doi.org/10.1144/0016-764904-071.

Hoke, G.D., Isacks, B.L., Jordan, T.E., Yu, J.S., 2004. Groundwater sapping origin for the giant quebradas of northern Chile. Geology 32 (7), 605–608.

Hoke, G.D., Isacks, B.L., Jordan, T.E., Blanco, N., Tomlinson, A.J., Ramezani, J., 2007. Geomorphic evidence for post-10 Ma uplift of the western flank of the central Andes 18°30′–22°S. Tectonics 26, 17. http://dx.doi.org/10.1029/2006TC002082.

Houston, J., Hartley, A.J., 2003. The central Andean west-slope rainshadow and its potential contribution to the origin of hyper-aridity in the Atacama Desert. Int. J. Climatol. 23, 1453–1464. http://dx.doi.org/10.1002/joc.938.

Jordan, T.E., Nester, P.L., Blanco, N., Hoke, G.D., Dávila, F., Tomlinson, A.J., 2010. Uplift of the Altiplano–Puna plateau: a view from the west. Tectonics 29, TC5007. http://dx.doi.org/10.1029/2010TC002661.

Kirk-Lawlor, N., Jordan, T.E., Rech, J.A., Lehmann, S., 2013. Late Miocene to Early Pliocene paleohydrology and landscape evolution of Northern Chile, 19° to 20°S. Palaeogeogr. Palaeoclimatol. Palaeoecol. 387, 76–90.

Kober, F., Schlunegger, F., Zeilinger, G., Scheider, H., 2006. Surface uplift and climate change: the geomorphic evolution of the Western Escarpment of the Andes of northern Chile between the Miocene and present. In: Spec. Pap., Geol. Soc. Am., vol. 398, pp. 75–86.

Kober, F., Ivy-Ochs, S., Schlunegger, F., Baur, H., Kubik, P., Wieler, R., 2007. Denudation rates and a topography-driven rainfall threshold in northern Chile: multiple cosmogenic nuclide data and sediment yield budgets. Geomorphology 83, 97–120. http://dx.doi.org/10.1016/j.geomorph.2006.06.029.

McQuarrie, N., 2002. The kinematic history of the central Andean fold-thrust belt, Bolivia: implications for building a high plateau. Geol. Soc. Am. Bull. 114 (8), 950–963. http://dx.doi.org/10.1130/0016-7606(2002)114<0950:tkhotc>2.0.co;2.

Mortimer, C., Saric, R.N., 1975. Cenozoic studies in northernmost Chile. Geol. Rundsch. 64, 395–420.

Mulch, A., Uba, C.E., Strecker, M.R., Schoenberg, R., Chamberlain, C.P., 2010. Late Miocene climate variability and surface elevation in the central Andes. Earth Planet. Sci. Lett. 290, 173–182. http://dx.doi.org/10.1016/j.epsl.2009.12.019.

Naranjo, J.A., Paskoff, R., 1985. Evolución cenozoica del piedemonte andino en la Pampa del Tamarugal, norte de Chile (18°–21°S). In: IV Congreso Geologico Chileno, vol. 4. Universidad del Norte de Chile, pp. 5-149–5-165.

Nishiizumi, K., Caffee, M., Finkel, R., Brimhall, G., 2005. Remnants of a fossil alluvial fan landscape of Miocene age in the Atacama Desert of northern Chile using cosmogenic nuclide exposure age dating. Earth Planet. Sci. Lett. 237, 499–507. http://dx.doi.org/10.1016/j.epsl.2005.05.032.

Oncken, O., Chong, G., Franz, G., Giese, P., Gotze, H., Ramos, V., Strecker, M., 2006. Deformation of the central Andean plate system – facts, fiction and constraints for plateau models. In: The Andes – Active Subduction Orogeny. Springer, Berlin, Heidelberg, pp. 3–27.

Rech, J., Currie, B., Michalski, G., Cowan, A., 2006. Neogene climate change and uplift in the Atacama Desert, Chile. Geology 34 (9), 761–764.

Roering, J.J., Kirchner, J.W., Dietrich, W.E., 1999. Evidence for non-linear, diffusive sediment transport on hillslopes and implications for landscape morphology. Water Resour. Res. 35, 853–870.

Schildgen, T., Hodges, K., Whipple, K., Reiners, P., Pringle, M., 2007. Uplift of the western margin of the Andean plateau revealed from canyon incision history, southern Peru. Geology 35, 523–526. http://dx.doi.org/10.1130/G23532A.1.

Schildgen, T.F., Hodges, K.V., Whipple, K.X., Pringle, M.S., van Soest, M.C., Cornell, K., 2009. Late Cenozoic structural and tectonic development of the western margin of the central Andean Plateau in southwest Peru. Tectonics 28, TC4007. http://dx.doi.org/10.1029/2008TC002403.

Schildgen, T.F., Balco, G., Shuster, D.L., 2010. Canyon incision and knickpoint propagation recorded by apatite $^{4}He/^{3}He$ thermochronometry. Earth Planet. Sci. Lett. 293 (3–4), 377–387. http://dx.doi.org/10.1016/j.epsl.2010.03.009.

Schlunegger, F., Zeilinger, G., Kounov, A., Kober, F., Husser, B., 2006. Scale of relief growth in the forearc of the Andes of Northern Chile (Arica latitude, 18°S). Terra Nova 18, 217–223. http://dx.doi.org/10.1111/ter.2006.18.issue-3.

Schlunegger, F., Kober, F., Zeilinger, G., von Rotz, R., 2010. Sedimentology-based reconstructions of paleoclimate changes in the Central Andes in response to the uplift of the Andes, Arica region between 19 and 21°S latitude, northern Chile. Int. J. Earth Sci. 99 (Suppl. 1), 123–137. http://dx.doi.org/10.1007/s00531-010-0572-8.

Sillitoe, R.H., McKee, E.H., 1996. Age of Supergene oxidation and enrichment in the Chilean porphyry copper province. Econ. Geol., Bull. Soc. Econ. Geol. 91 (1), 164–179.

Stock, J.D., Montgomery, D.R., 1999. Geologic constraints on bedrock river incision using the stream power law. J. Geophys. Res. 104, 4983–4993. http://dx.doi.org/10.1029/98JB02139.

Strecker, M., Alonso, R., Bookhagen, B., Carrapa, B., 2007. Tectonics and climate of the southern central Andes. Annu. Rev. Earth Planet. Sci. 35, 747–787. http://dx.doi.org/10.1146/annurev.earth.35.031306.140158.

Thouret, J.-C., Wörner, G., Gunnell, Y., Singer, B., Zhang, X., Souriot, T., 2007. Geochronologic and stratigraphic constraints on canyon incision and Miocene uplift of the Central Andes in Peru. Earth Planet. Sci. Lett. 263 (3–4), 151–166. http://dx.doi.org/10.1016/j.epsl.2007.07.023.

Tucker, G.E., Bras, R.L., 2000. A stochastic approach to modeling the role of rainfall variability in drainage basin evolution. Water Resour. Res. 36 (7), 1953–1964.

Tucker, G.E., Slingerland, R.L., 1994. Erosional dynamics, flexural isostasy, and long-lived escarpments: a numerical modeling study. J. Geophys. Res. 99, 12229–12243.

Uba, C.E., Strecker, M.R., Schmitt, A.K., 2007. Increased sediment accumulation rates and climatic forcing in the central Andes during the late Miocene. Geology 35, 979–982. http://dx.doi.org/10.1130/G224025A.1.

Victor, P., Oncken, O., Glodny, J., 2004. Uplift of the western Altiplano plateau: evidence from the Precordillera between 20° and 21°S (northern Chile). Tectonics 23, Tc4004. http://dx.doi.org/10.1029/2003TC001519.

Von Rotz, R., Schlunegger, F., Heller, F., Villa, I., 2005. Assessing the age of relief growth in the Andes of northern Chile: magneto-polarity chronologies from Neogene continental sections. Terra Nova 17, 462–471. http://dx.doi.org/10.1111/j.1365-3121.2005.00634.x.

Whittaker, A.C., 2012. How do landscapes record tectonics and climate? Lithosphere 4, 160–164. http://dx.doi.org/10.1130/RF.L003.1.

Willgoose, G.R., Bras, R.L., Rodriguez-Iturbe, I., 1991. A physically based coupled network growth and hillslope evolution model: 1. Theory. Water Resour. Res. 27 (7), 1671–1684.

Zeilinger, G., Schlunegger, F., Simpson, G., 2005. The Oxaya anticline (northern Chile): a buckle enhanced by river incision? Terra Nova 17, 368–375. http://dx.doi.org/10.1111/j.1365-3121.2005.00622.x.